INTERNATIONAL JOURNAL FOR NUMERICAL METHODS IN FLUIDS, VOL. 23, 1289–1310 (1996)

NUMERICAL PREDICTION OF TWO-PHASE FLOW IN BUBBLE COLUMNS

N. BOISSON

Rhône Poulenc Industrialisation, CRIT, 24 Avenue Jean Jaures, F69-153 Decines Charpieu Cedex, France

AND

M. R. MALIN

CHAM Limited, Bakery House, 40 High Street, Wimbledon, London SW19 5AU, U.K.

SUMMARY

A numerical model is described for the prediction of turbulent continuum equations for two-phase gas–liquid flows in bubble columns. The mathematical formulation is based on the solution of each phase. The two-phase model incorporates interfacial models of momentum transfer to account for the effects of virtual mass, lift, drag and pressure discontinuities at the gas–liquid interface. Turbulence is represented by means of a two-equation k–ε model modified to account for bubble-induced turbulence production. The numerical discretization is based on a staggered finite-volume approach, and the coupled equations are solved in a segregated manner using the IPSA method. The model is implemented generally in the multipurpose PHOENICS computer code, although the present appllications are restricted to two-dimensional flows. The model is applied to simulate two bubble column geometries and the predictions are compared with the measured circulation patterns and void fraction distributions.

KEY WORDS: bubble columns; computational fluid dynamics; turbulent two-phase flow

1. INTRODUCTION

Bubble columns are commonly used in the biochemical and petrochemical industries for a number of important industrial processes. A bubble column comprises a vessel filled with liquid, usually with a sparger ring located at or near the base of the column for dispersing the gas. In some configurations a draft tube is used to direct recirculation of the liquid and to influence the bubble motion. The need for more reliable and improved designs has led in recent years to the development of a number of mathematical models. The different types of model have been summarized by Svendsen and co-workers[1,2] and Celik and Wang.[3] The most complex models are those using computational fluid dynamics (CFD), by which is meant models based on numerical finite volume techniques. CFD models of bubble columns have been developed and applied by Svendsen and co-workers,[1,2] Huang[4] and Petersen.[5] All these models are based on a two-fluid modelling approach in which phasic continuum conservation equations are used in conjunction with appropriate closure models for the interfacial transfer processes and turbulent transport.

CCC 0271–2091/96/121289–22

Received October 1995
Revised March 1996

Efficient and reliable numerical techniques[6–9] are now available for the numerical solution of the coupled two-fluid equations and so the incorporation of appropriate closure relations is the key issue for successful CFD simulations. The interfacial modelling for momentum transfer involves the provision of closure models to account for the effects of drag, lift, virtual mass and interfacial pressure. The turbulence modelling requires the introduction of a suitable turbulence model for closure of the turbulent Reynolds stresses.

The two-fluid model described in this paper is based largely on the Huang– Petersen model, but differs from it in a number of important respects. The closure models for the interfacial forces and Reynolds stresses are those used by Huang[4] and Petersen,[5] but the present model takes into account the additional production of turbulent kinetic energy due to bubble–liquid interactions. Furthermore, the Huang–Petersen model represents the turbulent dispersion of bubbles through a dispersion force in the phasic momentum equations,[10] whereas the present model employs a turbulent diffusion term in the phasic continuity equations. This practice is shared by the model of Svendsen and co-workers,[1,2] but it is much older, having been used in the previous decade by Spalding's group.[11,12]

The other major difference between the two models is that the Huang–Petersen simulations were performed using a two-dimensional version of the Harlow– Amsden solution method,[6,13] whereas the present study uses the interphase slip algorithm (IPSA) of Spalding.[7,8] The present two- phase model has been implemented generally in the multipurpose PHOENICS CFD code. Furthermore, the input files specifying the calculations have been deposited in the PHOENICS library of two-phase flow examples. The model is therefore now available for immediate activation in future work, as well as for other workers to repeat the calculations described in this paper.

The two-fluid model is validated by application to the bubble column geometries studied experimentally by Hills[14] and Svendsen and co-workers.[1,2] This exercise is complemented by additional validation studies against one-dimensional analytical solutions and the data of Seriwaza *et al.*[15] for two-phase bubbly flow in pipes.

The remainder of this paper is divided into three sections, respectively dealing with the mathematical model, the presentation and discussion of results and the main conclusions of this study.

2. MATHEMATICAL MODEL

2.1. Continuity equations

The phasic continuity equations take the form

$$\partial(\rho_k r_k)/\partial t + \nabla \cdot (\rho_k r_k \mathbf{U}_k) = \nabla \cdot (\rho_k D \nabla r_k), \tag{1}$$

where ρ_k is the density of phase k, r_k is the volume fraction of phase k, $\mathbf{U}_k$ is the velocity vector of phase k and D is the phase diffusion coefficient. The subscript k refers to the continuous phase 'c' (liquid) or the dispersed phase 'd' (gas).

The phase diffusion term represents the turbulent flux associated with correlations between fluctuating velocity and volume fraction. The flux is modelled via a gradient diffusion approximation with the diffusion coefficient D given by

$$D = \nu_t/\sigma_r, \tag{2}$$

where ν_t is the turbulent kinematic eddy viscosity and σ_r is the turbulent Schmidt number for volume fractions, which, unless stated otherwise, is assigned a value of unity. The turbulent viscosity is computed from a modified k–ε turbulence model as described later.

The mean global continuity equation is

$$r_d + r_c = 1, \tag{3}$$

where r_d and r_c are the volume fractions of the dispersed and continuous phases respectively.

2.2. *Momentum equations*

The phasic momentum equations are given by

$$\begin{aligned}\partial(\rho_k r_k \mathbf{U}_k)/\partial t + \nabla\cdot(\rho_k r_k \mathbf{U}_k \mathbf{U}_k) = {} & -r_k \nabla P_k + \nabla\cdot[r_k(\boldsymbol{T}_{v,k} + \boldsymbol{T}_{t,k})] \\ & + r_k \rho_k \mathbf{g} + (P_{ki} - P_k)\nabla r_k + \mathbf{M}_{d,k} + \mathbf{M}_{vm,k} + \mathbf{M}_{l,k} \\ & + \nabla\cdot(\rho_k D \mathbf{U}_k \nabla r_k),\end{aligned} \tag{4}$$

where P_k is the static pressure of phase k, P_{ki} is the static pressure of phase k at the interface, $\mathbf{g}$ is the gravitational acceleration, $\boldsymbol{T}_{v,k}$ and $\boldsymbol{T}_{t,k}$ are the viscous and turbulent stress tensors for phase k respectively and $\mathbf{M}_{vm,k}$, $\mathbf{M}_{d,k}$ and $\mathbf{M}_{l,k}$ are the interfacial forces per unit volume due to virtual mass effects, drag forces and lift forces respectively.

The stress tensors are given in incompressible form by

$$\boldsymbol{T}_{v,k} = 2\rho_k \nu_l \boldsymbol{D}_k, \qquad \boldsymbol{T}_{t,k} = 2\rho_k \nu_t \boldsymbol{D}_k, \tag{5}$$

where ν_l is the kinematic laminar viscosity of the continuous phase and $\boldsymbol{D}_k$ is the deformation tensor,

$$\boldsymbol{D}_k = 0{\cdot}5[\nabla \mathbf{U}_k + (\nabla \mathbf{U}_k)^+], \tag{6}$$

where the superscript '+' denotes that the transpose of the dyadic $\nabla \mathbf{U}_k$ is taken.

2.3. *Interfacial drag forces*

The interfacial drag forces per unit volume are given by

$$\mathbf{M}_{d,d} = F(\mathbf{U}_c - \mathbf{U}_d), \qquad \mathbf{M}_{d,c} = -F(\mathbf{U}_c - \mathbf{U}_d), \tag{7}$$

where $\mathbf{U}_d$ and $\mathbf{U}_c$ are the phase velocity vectors and F is the interphase drag coefficient,

$$F = 0{\cdot}75 C_d \rho_c r_d r_c V_s / D_b, \tag{8}$$

where C_d is a dimensionless drag coefficient, D_b is the bubble diameter and $V_s (\equiv \sqrt{(\mathbf{U}_r \cdot \mathbf{U}_r)})$ is the magnitude of the slip velocity vector $\mathbf{U}_r$, i.e. the total relative mean velocity vector between the two phases.

The dimensionless drag coefficient C_d varies as a function of bubble Reynolds number

$$Re = V_s D_b / \nu_l \tag{9}$$

and Weber number

$$We = \rho_c V_s D_b^2 / \sigma, \tag{10}$$

where σ is the surface tension, which is given a value of 0·072 N m^{-1} for air–water systems. The following correlations,[4,5,16] which are suitable for air bubbles rising in unfiltered water, are employed:

$$C_d = 16/Re \quad \text{for region 1 with } Re < 0{\cdot}49, \tag{11}$$

$$C_d = 20{\cdot}68/Re^{0{\cdot}643} \quad \text{for region 2 with } 0{\cdot}49 < Re < 100, \tag{12}$$

$$C_d = 6{\cdot}3/Re^{0{\cdot}385} \quad \text{for region 2B with } Re \gg 100. \tag{13}$$

However, if $Re \gg 100$ and $We > 8$,

$$C_d = 8/3, \quad \text{for region 5;} \tag{14}$$

otherwise, if $Re \gg 100$ and $Re > 2065 \cdot 1/We^{2 \cdot 6}$,

$$C_d = We/3 \quad \text{for region 4.} \tag{15}$$

The region numbers correspond to Figure 1 in the paper of Kuo and Wallis[16] and are discussed in detail by Wallis.[17] For spherical bubbles, C_d is a function of Re only, whereas when bubbles become very distorted, C_d is a function of We only.

2.4. *Virtual mass forces*

The significance of the virtual mass term in the momentum equations is that it represents the force required to accelerate the apparent mass of the surrounding continuous phase in the immediate vicinity of the dispersed phase. These effects can be neglected if $\rho_d/\rho_c \gg 1$. For solid particles and liquid droplets in gases these effects are small, but they are important in the motion of gas bubbles through liquids.

Formulations of the virtual mass terms have been proposed by a number of workers.[18,19] The present study employs the Drew–Lahey formulation[19]

$$\mathbf{M}_{vm,c} = \rho_c C_{vm} r_d \mathbf{a}_{vm}, \qquad \mathbf{M}_{vm,d} = -\rho_c C_{vm} r_d \mathbf{a}_{vm}, \tag{16}$$

where C_{vm} is the virtual mass coefficient and $\mathbf{a}_{vm}$ is the virtual mass acceleration vector,

$$\mathbf{a}_{vm} = \partial(\mathbf{U}_d - \mathbf{U}_c)/\partial t + \mathbf{U}_d \cdot \nabla \mathbf{U}_d + \mathbf{U}_c \cdot \nabla \mathbf{U}_c. \tag{17}$$

The coefficient C_{vm} describes the volume of displaced fluid that contributes to the effective mass of the dispersed phase. In general this parameter is likely to be a function of r_d, but it is often taken as constant. For example, C_{vm} takes a value of 0·5 for spherical bubbles and different values for other shapes.[10,20]

In the present work, C_{vm} is calculated from[4,5,21]

$$C_{vm} = C_{vma}(1 \cdot 0 - 2 \cdot 78\langle 0 \cdot 2, r_d \rangle), \tag{18}$$

where $C_{vma} = 0 \cdot 5$ and $\langle a, b \rangle$ denotes that the minimum of a and b is taken. Provision is also made for constant values of C_{vm} to be used, as well as taking $C_{vm} = C_{vma} r_c$.[22]

2.5. *Interfacial lift forces*

Interfacial lift forces are particularly important for the prediction of phase separation and phase distribution phenomena. As an example, the lateral phase distribution for fully developed bubbly flow through a circular duct shows that bubbles accumulate near the walls for upward flow and near the centre of the duct for downward flow.[10,15,20,23]

The modelling of these lift forces has been considered by a large number of workers.[4,5,10,19,20,23–26] Following these researchers, the following expressions are used for the interfacial lift forces per unit volume:

$$\mathbf{M}_{l,c} = C_l \rho_c r_d (\mathbf{U}_d - \mathbf{U}_c) \times (\nabla \times \mathbf{U}_c), \qquad \mathbf{M}_{l,d} = -C_l \rho_c r_d (\mathbf{U}_d - \mathbf{U}_c) \times (\nabla \times \mathbf{U}_c), \tag{19}$$

where C_l is the interfacial lift coefficient. There is much uncertainty in the literature concerning the value of C_l. For example, Lahey and co-workers[10,20] report values in the range 0·01–0·5.

In the present work the lift coefficient C_l is computed from[4,5,19]

$$C_l = C_{la}(1 \cdot 0 - 2 \cdot 78\langle 0 \cdot 2, r_d \rangle), \tag{20}$$

where $C_{la} = C_{vma} = 0{\cdot}5$. The present implementation also allows for constant values of C_l, as well as for values to be computed from $C_l = C_{la} r_c$, as proposed by Watanabe *et al.*[22]

Following other workers,[1,2,4,5] negative values of C_l are employed in the present bubble column simulations. The justification for using negative lift coefficients has been discussed at great length by Svendsen *et al.*[2] and so this discussion will not be reiterated here. Suffice to say that Svendsen *et al.* claim that there is experimental evidence on the negative Magnus effect to support this practice, which also leads to successful predictions.

2.6. *Interfacial pressure forces*

The form of the pressure terms in the momentum equations (4) is taken from References 27 and 28. The usual practice in two-phase flow calculations is to assume that there are no pressure differences,[1,2]

$$P_k = P_{ki} = P, \tag{21}$$

so that the pressure terms $\mathbf{M}_{p,k} (\equiv -r_k \nabla P_k + (P_{ki} - P_k) \nabla r_k)$ in the momentum equations reduce to the familiar expression

$$\mathbf{M}_{p,k} = -r_k \nabla P. \tag{22}$$

This assumption is adequate in applications which do not involve acoustic effects or bubble expansion or contraction.[28]

The original pressure terms allow for the possibility of momentum transfer due to pressure discontinuities between the bulk phases and the interface. These effects may be included in the momentum equations by one of two alternative formulations of the interfacial pressure terms. The first is the one described by Huang,[4] Lahey *et al.*[10] and Petersen,[5] which will be referred to as the Lahey formulation. The second is the one described by Stuhmiller[29] and Prakash,[23] which will be referred to as the Stuhmiller formulation.

The Lahey formulation employs the pressure relationships

$$P_{di} - P_d = 0, \tag{23}$$

$$P_{ci} - P_c = -C_p \rho_c V_s^2, \tag{24}$$

$$P_{di} - P_{ci} = 2\sigma\zeta, \tag{25}$$

where ζ is the mean curvature and C_p is an empirical pressure coefficient defined below. Equation (24) represents a Bernoulli effect in the continuous phase flow field whereby the pressure on the liquid side of the interface is less than the bulk liquid pressure due to the velocity increase associated with the deflection of the flow around the dispersed bubbles. If the surface tension is presumed uniform and equations (23)–(25) are substituted into the momentum equation (4), the following pressure terms appear in the phasic momentum equations:

$$\mathbf{M}_{p,c} = -r_c \nabla P_c + C_p \rho_c V_s^2 \nabla r_d, \tag{26}$$

$$\mathbf{M}_{p,d} = -r_d \nabla P_c + r_d \nabla (C_p \rho_c V_s^2). \tag{27}$$

The Stuhmiller formulation employs relations (24) and (25) above, together with

$$P_d - P_c = 2\sigma\zeta, \tag{28}$$

which implies $P_{di} - P_d = P_{ci} - P_c$ rather than $P_{di} - P_d = 0$ as used in the Lahey formulation. If the surface tension is presumed uniform and equations (24), (25) and (28) are substituted into the momentum equation (4), the following pressure terms appear in the momentum equations:

$$\mathbf{M}_{p,c} = -r_c \nabla P_c + C_p \rho_c V_s^2 \nabla r_d, \tag{29}$$

$$\mathbf{M}_{p,d} = -r_c \nabla P_c - C_p \rho_c V_s^2 \nabla r_d. \tag{30}$$

The present implementation makes provision for using both these formulations, although only the Lahey formulation is used in the present applications.

Lahey *et al.*[10] report values of C_p in the range 0·25–1·0, whereas Huang[4] and Petersen[5] take

$$C_p = C_{pa}(1 + r_d) r_c^2 \tag{31}$$

and Antal *et al.*[30] take $C_p = C_{pa} r_c$, with $C_{pa} = 0{\cdot}25$ in both cases.

The present study uses equation (31), although the model implementation also makes provision for constant values as well as the proposal of Antal *et al.*[30]

2.7. *Turbulence modelling*

The turbulence is assumed to be a property of the continuous phase and so the turbulent kinematic viscosity ν_t is shared by both phases. The turbulent dynamic viscosity of each phase is then calculated by multiplying ν_t by the phasic density. This treatment is in accordance with the neglect of internal flow inside the dispersed phase.

The turbulent viscosity is determined from the solution of modelled transport equations for the turbulent kinetic energy k and its dissipation rate ε. For two-phase high-Reynolds-number turbulent flows the following modified form of the k–ε model is employed:

$$\partial(\rho_c r_c k)/\partial t + \nabla \cdot (\rho_c r_c \mathbf{U}_c k) = \nabla \cdot [\rho_c r_c (\nu_l + \nu_t/\sigma_k) \nabla k] + \rho_c r_c (P_k - \epsilon) + \nabla \cdot [\rho_c (\nu_t/\sigma_r) k \nabla r_c] + r_c P_b, \tag{32}$$

$$\partial(\rho_c r_c \epsilon)/\partial t + \nabla \cdot (\rho_c r_c \mathbf{U}_c \epsilon) = \nabla \cdot [\rho_c r_c (\nu_l + \nu_t/\sigma_\epsilon) \nabla \epsilon] + r_c c_{1\epsilon} P_b \epsilon/k + (\rho_c r_c \epsilon/k)(C_{1\epsilon} P_k - C_{2\epsilon} \epsilon) + \nabla \cdot [\rho_c (\nu_t/\sigma_r) \epsilon \nabla r_c]. \tag{33}$$

$$\nu_t = C_\mu k^2/\epsilon, \tag{34}$$

where P_k is the volumetric production rate of k by shear forces,

$$P_k = 2\nu_t \mathbf{D}_c : \nabla \mathbf{U}_c, \tag{35}$$

and P_b is the production rate of k due to the drag work that the bubbles do as they move through the liquid,

$$\mathbf{P}_b = \mathbf{C}_b F \mathbf{U}_r \cdot \mathbf{U}_r, \tag{36}$$

with C_b an empirical constant denoting the fraction of bubble-induced turbulence going into the large-scale turbulence of the liquid phase.

The bubble-induced turbulence production terms, which have been used by several other workers,[2,31,32] attempt to allow for the additional production and dissipation of turbulence due to the presence of the bubbles. In general, large bubbles may be expected to enhance turbulence, whereas small bubbles may be expected to suppress turbulence. The present work uses values of C_b in the range 0·01–0·05, which is comparable with the value of 0·02 used for two-phase bubbly flow in conduits.[32]

The values used for the other model constants are those recommended by Launder and Spalding,[33] namely $\sigma_k = 1{\cdot}0$, $\sigma_\epsilon = 1{\cdot}314$, $C_\mu = 0{\cdot}09$, $C_{1\epsilon} = 1{\cdot}44$ and $C_{2\epsilon} = 1{\cdot}92$.

2.8. *Boundary and initial conditions*

In the present work the flow can be bounded by an inflow boundary, an outflow boundary, a solid wall and a symmetry plane. The inflow conditions, and the initial conditions in transient simulations, depend on the flow considered and therefore their definition for each problem will be deferred until Section 3.

Although laminar transport has been allowed for in the k–ε model, it is not applicable near walls where the turbulence Reynolds number is low. In these regions, equilibrium wall functions[34] are used in boundary conditions which are specified at a grid point located in the fully turbulent regime. At this point the logarithmic law of the wall prevails and the turbulence is assumed to be in local equilibrium. This practice leads to the calculation of the carrier phase wall shear stress in terms of the dimensionless wall distance $y^+(= U^*\delta/\nu_l)$ and logarithmic law constants κ ($=0{\cdot}41$) and E ($=8{\cdot}6$). The wall shear stress is taken as zero for the dispersed phase. The boundary conditions for k and ε are specified at the near-wall grid point in terms of the friction velocity $U*$ and the wall distance δ.

At symmetry planes, such as the axis of a pipe, the normal gradients for all dependent variables are zero, so that a zero-flux condition is applied along such boundaries. At outflow boundaries the static pressure is specified and held constant, so that the volume fractions and mass outflows of the selected phases result as part of the overall solution.

2.9. *Solution of equations*

The foregoing mathematical model has been incorporated for general use into the commercial CFD code PHOENICS. The implementation is general in that it is applicable to steady or unsteady, one-, two- or three-dimensional turbulent or laminar flows using Cartesian, cylindrical polar or curvilinear co-ordinates.

The numerical procedure used is of the finite volume type in which the original partial differential equations are converted into algebraic finite volume equations with the aid of discretization assumptions. For this purpose the solution domain is subdivided into a number of control volumes using a conventional staggered grid approach. The volume fractions, scalar variables and pressure are stored at the grid nodes, while the velocities are stored at staggered locations which lie between the pressure nodes. The control volumes for the velocities are staggered in relation to the control volumes for other variables.

The finite volume equations for each variable are derived by integrating the partial differential equations over each control volume. Fully implicit backward differencing is employed for the transient terms and central differencing for the diffusion terms. The convection terms are discretized using hybrid differencing in which the convective terms are approximated by central differences if the cell face Peclet number $Pe \leqslant 2$ and by upwind differences if $Pe > 2$. At faces where the upwind scheme is used, physical diffusion is omitted altogether. The integration procedure results in a coupled set of algebraic finite volume equations which express the value of a variable at a grid node in terms of the values at neighbouring grid points and the nodal value at the old time level.

The finite volume equations are solved iteratively using the SIMPLEST[11] and IPSA algorithms of Spalding,[7,8] which are embodied in the PHOENICS code for use in both parabolic and elliptic modes of calculation. The calculation procedure is organized in a slab-by-slab manner in which all dependent variables are solved at the current slab before attention moves to the next higher slab. The slabs are thus visited in turn, from the lowermost to the uppermost, and a complete series of slab visits is referred to as a sweep through the solution domain. For parabolic calculations, only one such sweep is required, with many iteration cycles at each slab, and no outflow boundary condition is required as this is an outcome of the solution. For elliptic calculations, many such sweeps are

conducted until convergence is attained at the current time level; in addition, the pressure equation is solved in a simultaneous whole-field manner at the end of each sweep. Thereafter the solution proceeds to the next time level where the iterative process is repeated.

The numerical solution procedure requires appropriate relaxation of the flow variables in order to procure convergence. Two types of relaxation are employed, namely inertial and linear. The former is normally applied to the velocity variables, whereas the latter is applied to all other flow variables, as and when necessary.

The convergence requirement is that for each set of finite volume equations the sum of the absolute residual sources over the whole solution domain is less than 1 per cent of reference quantities based on the total inflow of the variable in question. An additional requirement is that the values of monitored dependent variables at a selected location do not change by more than 0·1 per cent between successive iteration cycles.

3. APPLICATIONS

3.1. Testing

The correctness of the interfacial drag and virtual mass models was tested separately by reference to one-dimensional calculations which may be compared with analytical solutions. These comparisons are not given here because of space limitations, but the interested reader is referred to Reference 35 for the detailed comparisons.

The first test case concerned a cloud of air bubbles rising steadily through stagnant water. After a relatively short period of acceleration the bubbles attain a uniform terminal velocity under which the drag force balances the buoyancy force. The drag model was validated successfully by calculating the terminal rise velocity for each of the five different flow regions of the Kuo–Wallis[16] drag model.

The second case considered was the acceleration of bubbles by a uniform flowing gas stream. The analytical solution for this case has been given by Morsi and Alexander[36] and it is easily extended to include virtual mass effects. The test calculations employed a constant drag coefficient $c_d = 0{\cdot}44$ and a virtual mass coefficient $C_{vm} = 0{\cdot}5$. The virtual mass model was validated successfully by comparing the calculated and analytical distributions of the bubble velocity.

The final analytical case was the one-dimensional transient case documented by Hewitt *et al.*[37] Denser fluid initially rests above lighter fluid in a vertical tank 2 m high and then it falls down to the bottom under gravity whilst the lighter fluid rises to the top of the tank. Eventually, after a time period of about 10 s, all the dense phase rests on the bottom of the tank with the lighter phase at the top. The densities of the two fluids were chosen nearly equal ($\rho_c = 1$ and $\rho_d = 0{\cdot}999$) so as to allow comparisons with published analytical and numerical solutions.[37] The gravitational acceleration was defined by $g \equiv 0{\cdot}5(\rho_d + \rho_c)/(\rho_c - \rho_d)$ and the virtual mass coefficient was taken as $C_{vma} r_c$ with $C_{vma} = 1{\cdot}0$. The interfacial drag coefficient was calculated from $F = 2\rho_d r_c r_d$. The predicted distributions of the dense phase volume fraction at $t = 2$, 4, 6 and 8 s were found to be in reasonable agreement with the analytical solutions and very similar to other numerical results.[37]

3.2. Bubbly air–water flow in a pipe

As a precursor to bubble column flows, the problem considered is the prediction of radial phase distribution in turbulent bubbly air–water upflow in a pipe.[15] The Reynolds number based on superficial liquid velocity and pipe diameter D_p is 80,000. The inlet superficial gas and liquid velocities are $j_g = 0{\cdot}077$ m s^{-1} and $j_l = 1{\cdot}36$ m s^{-1}. The inlet void fracton is given by $j_g/(j_g + j_l)$, which presumes no slip between the incoming phases.

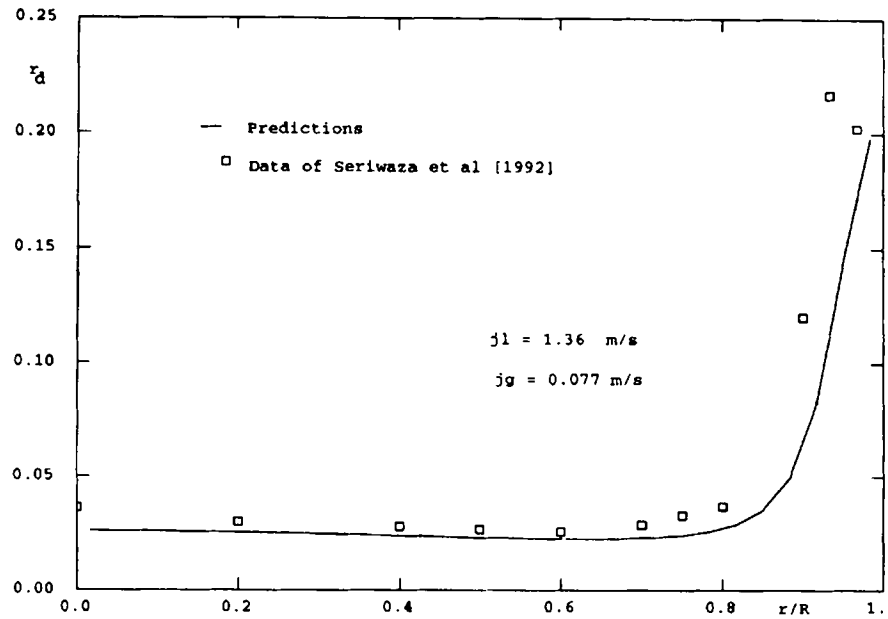

Figure 1. Seriwaza pipe upflow: void fraction radial profiles

The two-dimensional calculations are performed with the parabolic solution procedure on a cylindrical polar mesh with 30 uniformly distributed radial grid cells. The forward-marching integration is carried out with a forward step size $\Delta z = 0{\cdot}1D_p$ and the calculation is terminated 35 diameters downstream of the inlet. This location corresponds to the experimental measuring station which lies in the region of fully developed flow. Mesh refinement tests were carried out and little difference was obtained in the results when using 40 radial grid cells and $\Delta z = 0{\cdot}05D_p$.

The calculations are carried out with $C_{la} = 0{\cdot}075$, $C_{vma} = 0{\cdot}5$, $C_{pa} = 0{\cdot}25$ and $C_b = 0{\cdot}05$. The bubble diameter is taken as 3 mm,[15] while the fluid properties are taken as $\rho_l = 1000$ kg m^{-3}, $\rho_g = 1{\cdot}23$ kg m^{-3} and $\nu_l = 10^{-6}$ m^2 s^{-1}.

Figures 1 and 2 present the results in terms of measured and predicted radial profiles of the void fraction and vertical liquid velocity. The void fraction profile reveals that gas is taken away from the centre and towards the wall. The behaviour is due to the lift force driving the bubbles towards the wall in upflow. The predictions are in fairly good agreement with the data, although the near-wall peak is not reproduced by the model. It can also be seen that the model predictions of the liquid upflow velocity agree very well with the measurements. It should be mentioned that the present results are very similar to those reported by Lahey[20] with a somewhat different two-fluid model. In subsequent work, Lahey and Lopez de Bertodano[38] predicted the near-wall void peaking by introducing a somewhat geometry-specific near-wall lubrication-like force.

3.3. Hills bubble column

The case considered is the bubble column of Hills,[14] which provides detailed measurements of voidage distribution and liquid velocity at a position 0·6 m above the base of the column. The column has an internal diameter of 0·138 m and a height of 1·37 m. The column is initially completely filled with water and air enters at the base of the column through a sieve plate. Eventually the flow attains

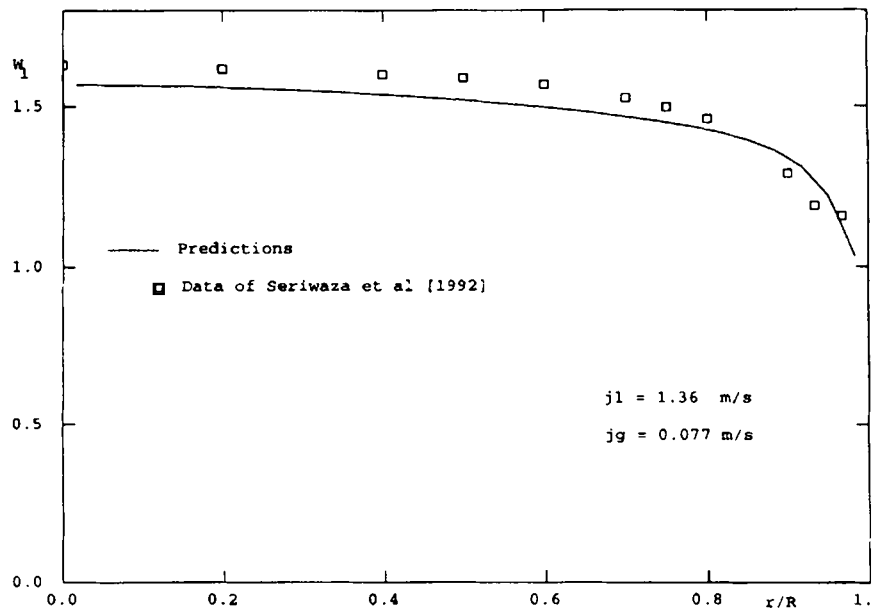

Figure 2. Seriwaza pipe upflow: vertical liquid velocity radial profiles

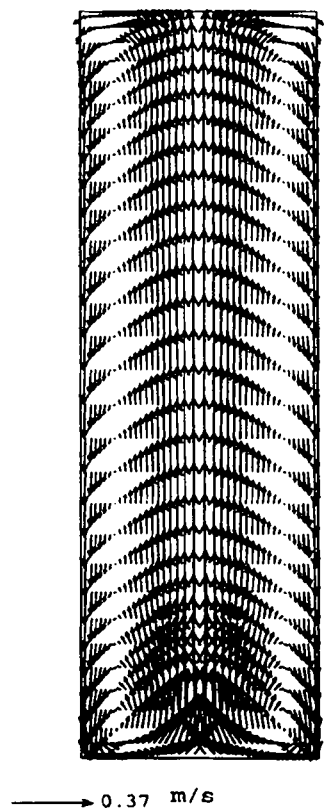

Figure 3. Hills bubble column: liquid phase velocity vectors (steady state solution; transient simulation)

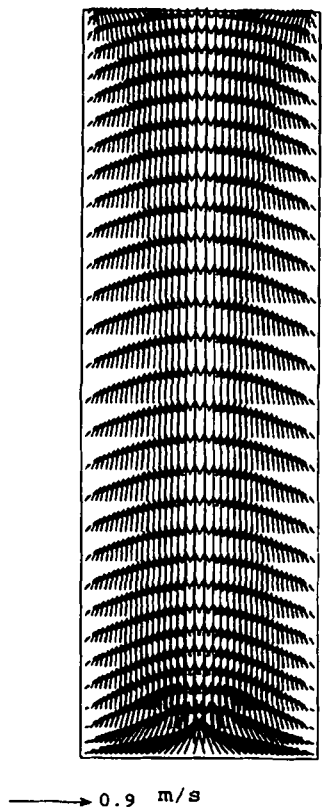

Figure 4. Hills bubble column: gas phase velocity vectors (steady state solution; transient simulation)

steady state conditions with gross circulation of the liquid in the column. The liquid is carried by the gas up the centre of the column and the liquid then turns through 180° at the top and descends down the outer wall.

Transient, two-dimensional axisymmetric calculations are performed on a cylindrical polar mesh with five different mesh sizes: 10 by 20, 15 by 20, 20 by 20, 20 by 30 and 20 radial grid cells by 40 vertical grid cells. The results indicated that a 20 by 30 mesh size gives a good compromise between the desired numerical accuracy and computational time. Increasing the number of radial mesh points from 15 to 20 had but a small effect on the results, as did increasing the number of vertical grid points from 30 to 40.

The calculation is started from a column filled with stagnant liquid and the liquid is then allowed to leave at the top of the column through a single fixed-pressure cell adjacent to the wall. The air is injected uniformly at the base of the column with a velocity of 0·038 m s^{-1}, resulting in a gas volume inflow rate of 2·046 m^3 h^{-1}. The air is allowed to leave at the top of the column via a fixed-pressure boundary located across the whole radial extent of the column. The bubble diameter is taken as 7·61 mm,[39] while the fluid properties are taken as $\rho_l = 1000$ kg m^{-3}, $\rho_g = 1{\cdot}23$ kg m^{-3} and $\nu_l = 10^{-6}$ m^2 s^{-1}.

Transient calculations are performed with $C_{la} = -0{\cdot}5$, $C_{vma} = 0{\cdot}5$, $C_{pa} = 0{\cdot}25$ and $C_b = 0{\cdot}01$. A time step of 0·05 s is employed with a maximum of 100 sweeps per time step. Steady state conditions are reached after about 20 s. Although strictly the problem needs to be run as a transient so as to

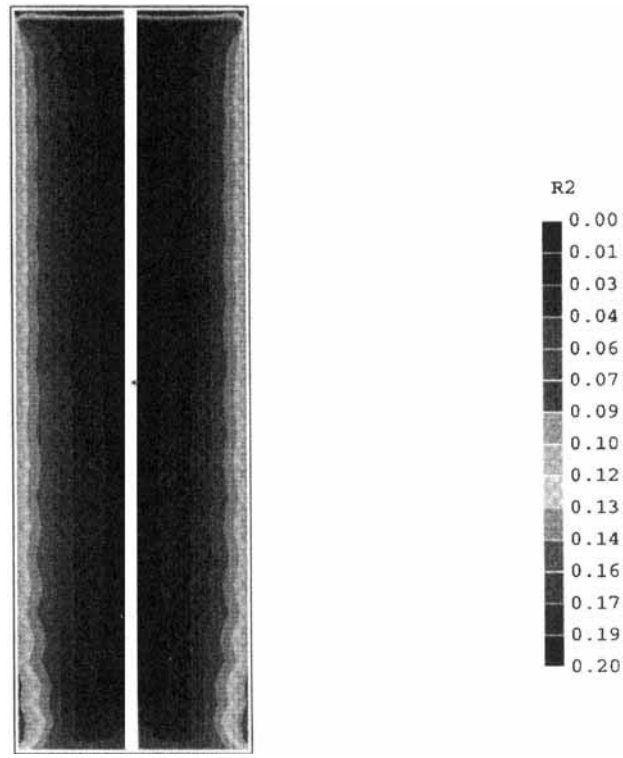

Figure 5. Hills bubble column: void fraction contours (steady state solution; transient simulation)

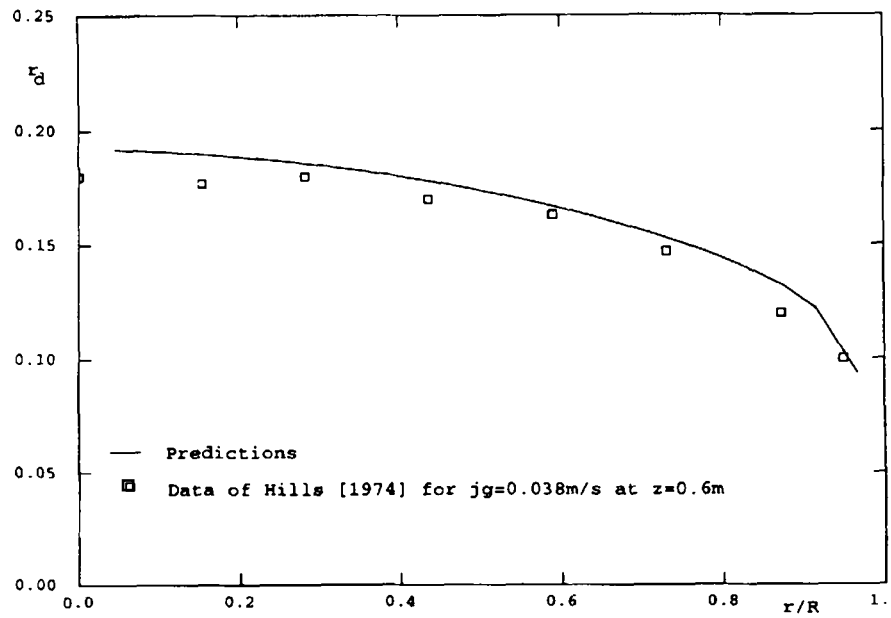

Figure 6. Hills bubble column: void fraction radial profiles

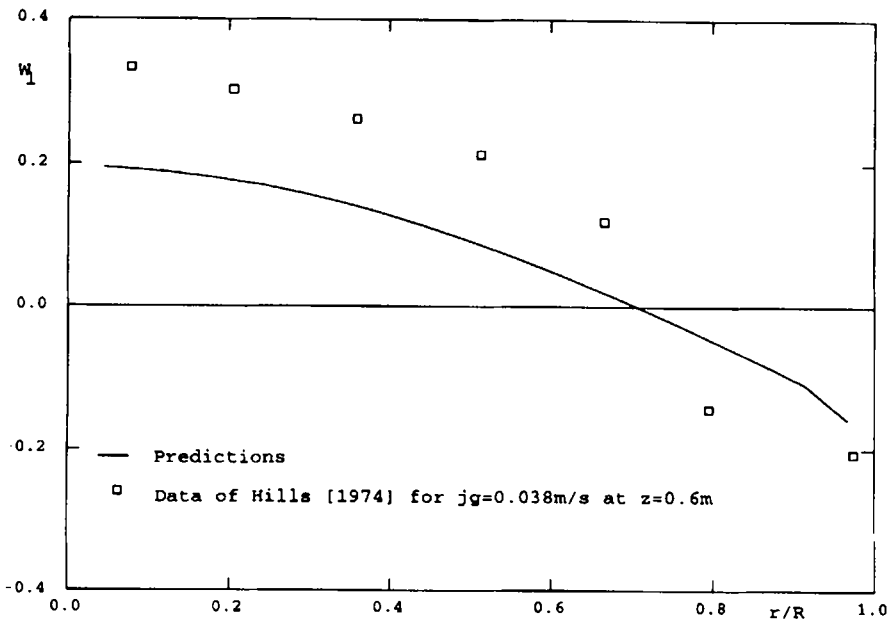

Figure 7. Hills bubble column: vertical liquid velocity radial profiles

specify the total liquid volume, a steady state calculations is also performed using the same boundary conditions as used in the transient simulation. The motivation for this calculation is computational economy.

Transient simulations. Steady state results are presented and discussed in this subsection and compared where possible with the measurements of Hills.[14] Figures 3–5 show liquid phase velocity vectors, gas phase velocity vectors and void fraction contours respectively. Figures 6 and 7 present the predicted and measured radial profiles of the void fraction and liquid phase vertical velocity at the measuring plane respectively.

The predicted flow patterns shown in Figures 3 and 4 for the two phases agree with those observed experimentally by Hills.[14] The clockwise liquid circulation is a consequence of the density difference produced by the non-uniform gas hold-up shown in Figure 5. The voidage predictions show low values at the walls and high values at the flow axis. This is in agreement with the experimental observations. It is important to note that in view of the uniform inflow of gas, the inclusion of the interfacial lift force is essential for producing radial phase distribution and hence liquid circulation.

The predicted gas hold-up of 0·15 for the entire column is in good agreement with the average value of 0·14 indicated by the measurements.[14] The comparisons between the void fraction profiles shown in Figure 6 confirm the quality of the predictions, with the model producing very good agreement with the data.

Figure 7 shows that the vertical liquid velocity is underestimated by the model. This discrepancy is also evident in the numerical results of Petersen,[5] who reported even lower values of the liquid velocity, e.g. about 0·1 m s^{-1} at the flow axis.

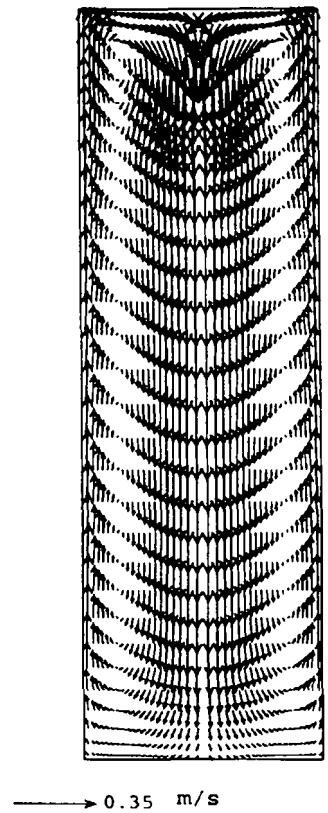

Figure 8. Hills bubble column: liquid phase velocity vectors (steady state simulation)

Steady simulations. The results of the steady state calculation are presented in Figures 8 and 9 in terms of the liquid phase velocity vectors and void fraction contours respectively. These figures show the striking result that converged solutions are obtained which exhibit opposite trends to those observed in the experiments and transient calculations. The results show that the liquid circulation is anticlockwise and that the void fraction is higher near the wall than at the flow axis. The predicted gas hold-up for the entire column agrees with the data and that predicted by the transient calculation.

These results may be explained by the fact that the interfacial lift model permits two numerical solutions, only one of which is physical. This was confirmed by (a) repeating the steady state calculation using the steady state transient solution as an initial starting field and (b) performing a transient calculation using the solution obtained from the steady state calculation as initial condition. Both these calculations maintained the initial solution fields, thereby confirming the existence of two solutions to the finite volume equations.

It is suggested here that the transient calculation produces the physical solution because this calculation includes transient virtual mass terms, whereas the steady state calculation does not. These forces may be expected to stabilize the system in the early stages of the transient, offering increased inertia to the bubble motion, thereby acting to resist any tendency for the lift forces to induce an anticlockwise liquid circulation.

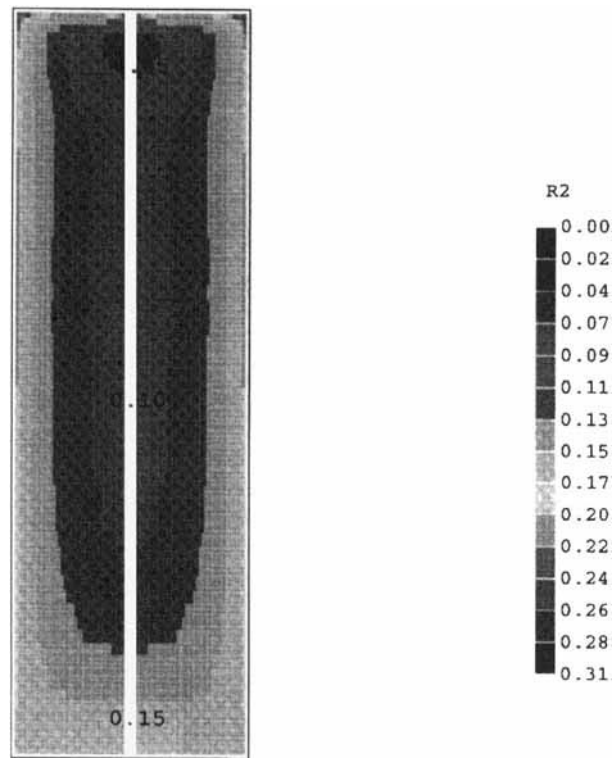

Figure 9. Hills bubble column: void fraction contours (steady state simulation)

3.4. *Trondheim bubble column*

The bubble column geometry is that described by Svendsen and co- workers.[1,2] The column is 4·25 m high with a diameter of 0·288 m. The media used are air and water, which enter uniformly and vertically at the bottom of the column. The bubble column operates at atmospheric pressure and both phases are allowed to leave at the top of the column. The experimental data reveal a gross liquid circulation pattern in which liquid upflow occurs at the flow axis and liquid downflow at the column walls. The inlet superficial velocities for the gas and liquid are $j_g = 0{\cdot}08$ m s^{-1} and $j_l = 0{\cdot}01$ m s^{-1}, so that the volume inflow rates of gas and water are 18·76 and 2·345 m^3 h^{-1} respectively. Svendsen and co- workers measured radial distributions of the void fraction, vertical liquid velocity and vertical velocity fluctuations at a station located 1·6 m above the inlet plane.

Two-dimensional axisymmetric calculations are performed on a cylindrical polar mesh with four different mesh sizes: 15 by 30, 25 by 30, 30 by 30 and 25 radial grid cells by 40 vertical grid cells. The computations indicated that a 25 by 30 mesh size produced results of sufficient numerical accuracy. The use of 30 rather than 25 radial mesh points produced little change in the results, as did increasing the number of vertical grid points from 30 to 40.

Following Torvik and Svendsen,[1] the inlet void fraction is taken as 0·2 and the gas and liquid inlet velocities are set to 0·4 and 0·0125 m s^{-1} respectively. A fixed-pressure boundary condition is applied to both continuity equations at the outlet boundary. The bubble diameter is taken as 10 mm, while the fluid properties are taken as $\rho_l = 1000$ kg m^{-3}, $\rho_g = 1{\cdot}19$ kg m^{-3} and $\nu_l = 10^{-6}$ m^2 s^{-1}.

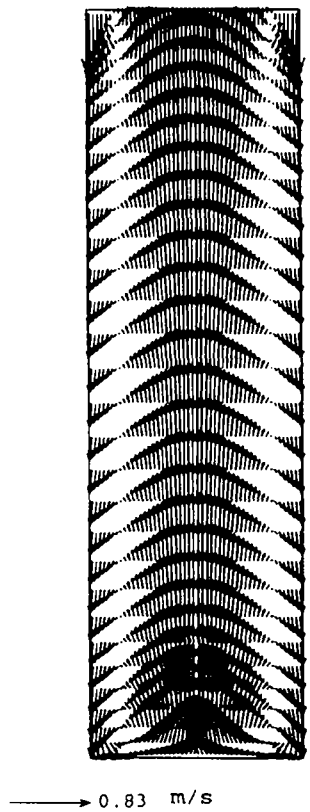

Figure 10. Trondheim bubble column: liquid phase velocity vectors

Numerical simulations are made with $C_l = -0{\cdot}5$, $\sigma_r = 1{\cdot}5$, $C_{vma} = 0{\cdot}5$, $C_{pa} = 0{\cdot}25$ and $C_b = 0{\cdot}05$. The use of a variable lift coefficient proved unsatisfactory for this application, as the predicted volume fraction profile at the measuring station was too flat. Evidently, more research is needed to predict both bubble column geometries with the same set of model coefficients.

Figures 10–13 show liquid phase velocity vectors, gas phase velocity vectors, void fraction contours and contours of the turbulent kinetic energy respectively. The computed and measured radial distributions of the void fraction, vertical liquid velocity and vertical velocity fluctuations at $z = 1{\cdot}6$ m are presented in Figures 14–16 respectively.

The velocity vectors in Figures 10 and 11 show fairly similar global recirculation patterns for the gas and liquid phases. The gas phase recirculation size is obviously much narrower, being restricted to a thin layer close to the wall. The radial lift force acts to drive the bubbles against the liquid phase vertical velocity gradients and so the void fraction contours depicted in Figure 12 show larger void fractions at the column centre than at the wall. This result is in agreement with experiment, as may be seen on inspection of Figure 14.

The comparisons between calculation and experiment made in Figures 14 and 15 show that the computations predict broadly the correct trends. The void fraction distributions displayed in Figure 14 reveal that the model produces good overall agreement with data. The calculation of total gas hold-up for the column is 0·28, but the experimenters did not report a value for comparison. Figure 15 reveals that the model produces very good agreement with the velocity data.

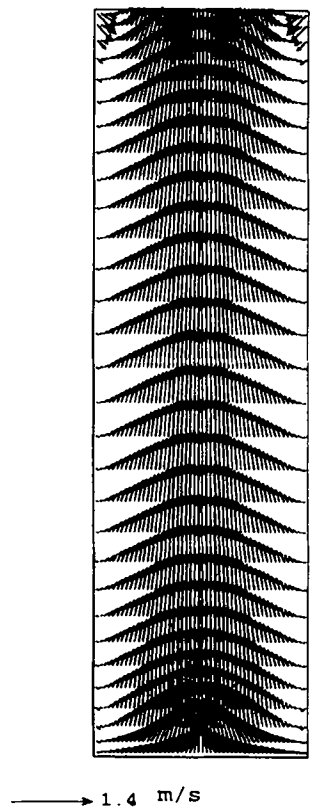

Figure 11. Trondheim bubble column: gas phase velocity vectors

Figure 16 shows that the predicted values of the vertical velocity fluctuations are lower than the measured values, a discrepancy that was also reported by Torvik and Svendsen[1] with a similar two-fluid model. The contours of turbulent kinetic energy presented in Figure 13 reflect the distribution observed in Figure 16, except that turbulence energy maxima are formed at the extremities of the column.

4. CONCLUDING REMARKS

A mathematical model has been described for the simulation of turbulent, two- phase gas–liquid flows in bubble columns. Turbulence was represented by means of a modified two-equation model which accounts for bubble-induced turbulence production. The turbulent dispersion of bubbles was modelled by a gradient diffusion term in the phasic continuity equations. The interfacial modelling comprised momentum transfer terms to account for the effects of drag, virtual mass, lift and interfacial pressure. The drag model takes into account the various bubble shape regimes encountered in two-phase bubbly flows.

The model has been validated by application to two laboratory bubble column geometries.[1,2,14] It has been shown that the model can predict the observed trends in phase distribution and relative velocity and the numerical solutions were found to be in encouraging agreement with most of the experimental data. Although future application to other bubble columns is feasible, the present study

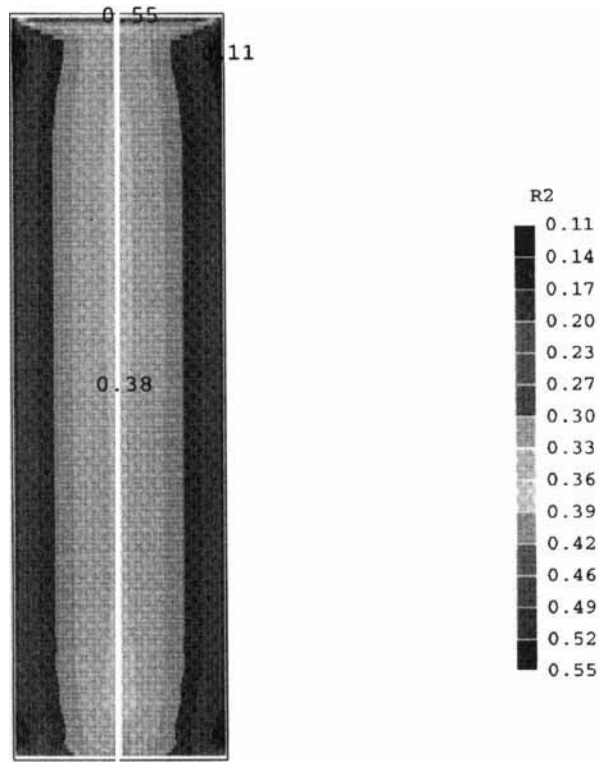

Figure 12. Trondheim bubble column: void fraction contours

has demonstrated that the values of the various model coefficients are by no means universal. Therefore the state of the physical modelling is such that much more research is needed before the model can be used as a reliable design tool for industrial bubble columns.

There are a number of ways in which the present two-fluid model can be improved to increase its capabilities and to provide more accurate numerical simulations. These include the introduction of closure models for the pressure–void correlations which appear in the statistically averaged momentum equations, the introduction of interphase heat and mass transfer, the investigation of flow regimes other than bubbly flow, the introduction of gas phase compressibility and, most importantly, the implementation of a model to account for variations in local bubble size due to fragmentation and coalescence.

ACKNOWLEDGEMENTS

This work was sponsored jointly by Rhône Poulenc Industrialisation and CHAM under contract C115. The authors would like to thank Dr. John Heritage and Mira Madhav of CHAM for their valuable discussions.

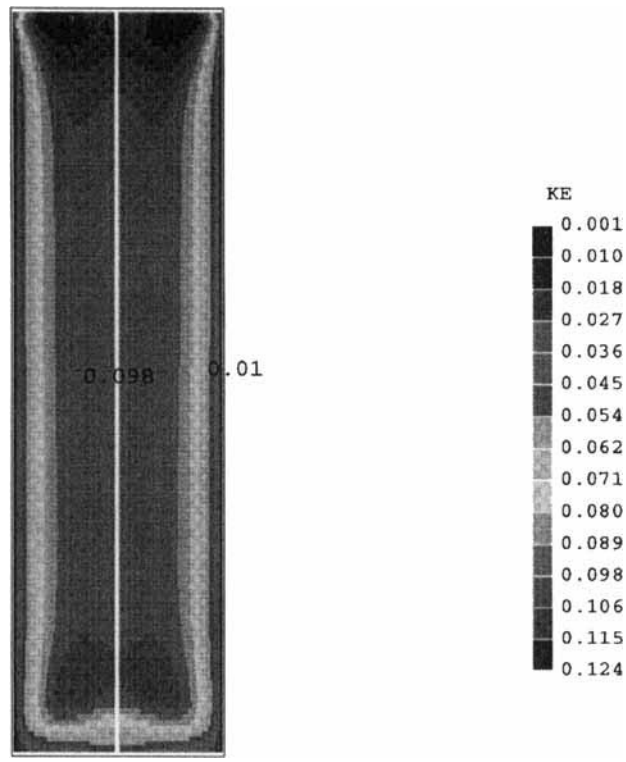

Figure 13. Trondheim bubble column: turbulent kinetic energy contours (J kg^{-1})

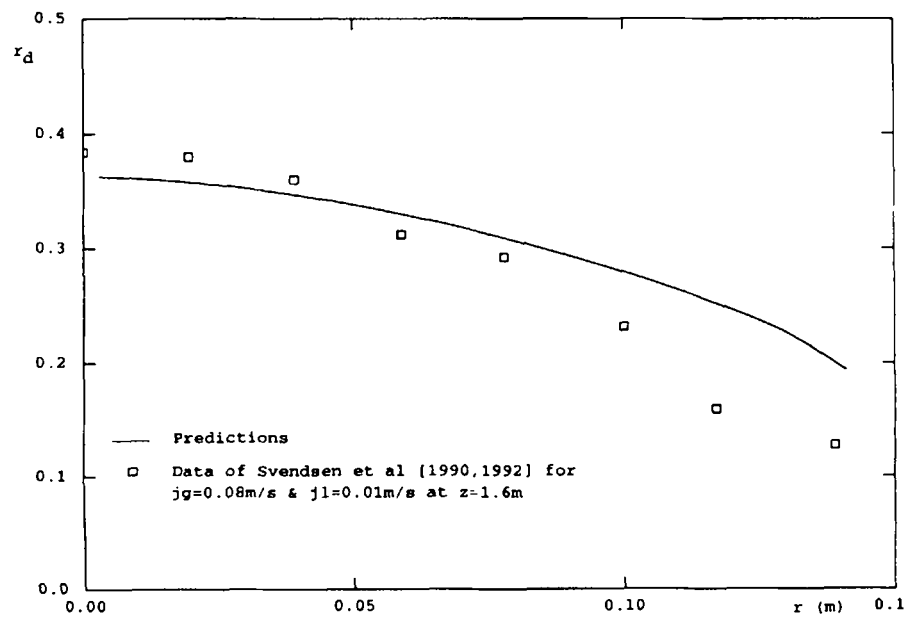

Figure 14. Trondheim bubble column: void fraction radial profiles

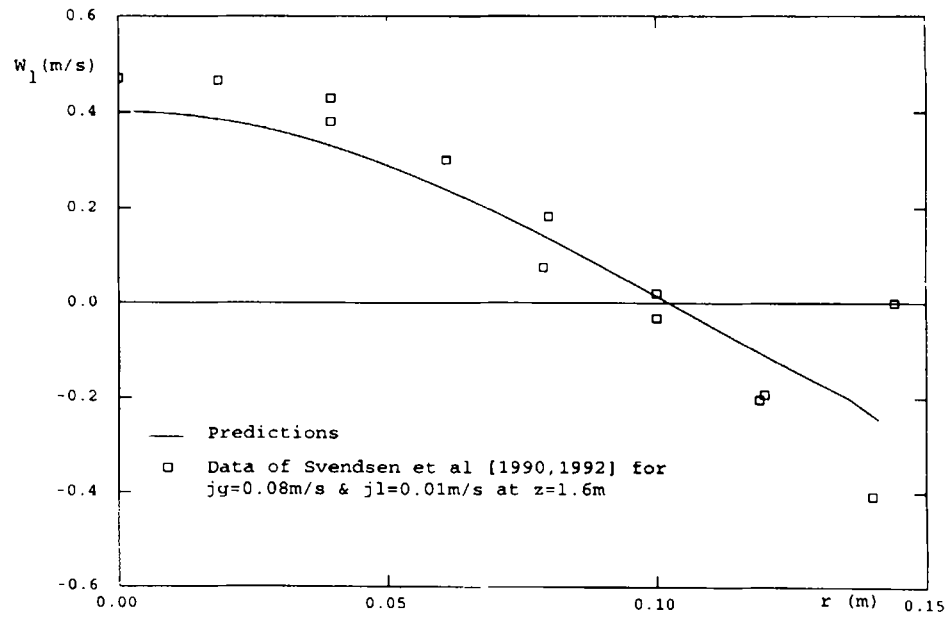

Figure 15. Trondheim bubble column: vertical liquid velocity radial profiles

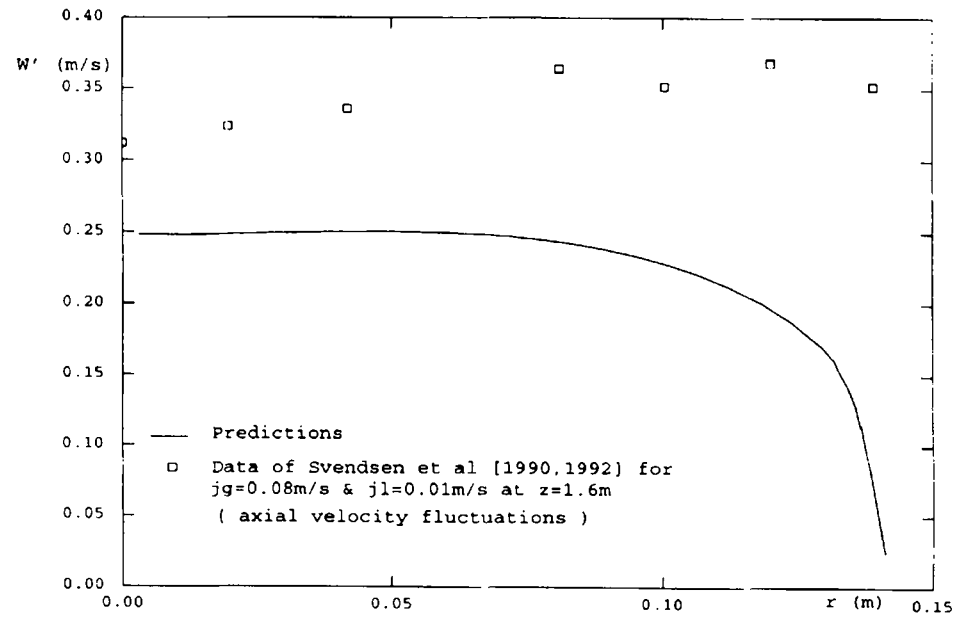

Figure 16. Trondheim bubble column: turbulent kinetic energy radial profiles

REFERENCES

1. R. Torvik and H. F. Svendsen, 'Modelling of slurry reactors; a fundamental approach', *Chem. Eng. Sci.*, **45**, 2325 (1990).
2. H. F. Svendsen, H. A. Jakobsen and R. Torvik, 'Local flow structures in internal loop and bubble-column reactors', *Chem. Eng. Sci.*, **47**, 3297 (1992).
3. I. Celik and Y. Z. Wang, 'Numerical simulation of liquid circulation in a bubbly column', in *Numerical Methods for Multiphase Flows*, FED Vol. 91, ASME, New York, 1990, p. 19.
4. B. Huang, 'Modelisation numerique d'ecoulements diphasiques a bulles dans de reacteurs chimiques', *Ph.D. Thesis*, Université Claude Bernard, Lyon, 1989.
5. K. O. Petersen, 'Etude experimentale et numerique des ecoulements diphasiques dans les reacteurs chimiques', *Ph.D. Thesis*, Université Claude Bernard, Lyon, 1992.
6. F. H. Harlow and A. A. Amsden, 'Numerical calculation of multiphase flow', *J. Comput. Phys.*, **17**, 19 (1975).
7. D. B. Spalding, 'The calculation of free-convection phenomena in gas-liquid mixtures', in N. Afgan and D. B. Spalding (eds), *Turbulent Buoyant Convection*, Hemisphere, Washington, DC, 1977, p. 569.
8. D. B. Spalding, 'Numerical computation of multiphase flow and heat transfer', in C. Taylor and K. Morgan (eds), *Recent Advances in Numerical Methods in Fluids*, Pineridge, Swansea, 1980, pp. 139–168.
9. S. Banerjee, 'Numerical methods', *Proc. Multiphase Flow and Heat Transfer: Bases, Modelling and Applications*, Zurich, March 1995.
10. R. T. Lahey, M. Lopez de Bertodano and O. C. Jones, 'Phase distribution in complex geometry ducts', *Nucl. Eng. Design*, **141**, 177 (1993).
11. D. B. Spalding and N. C. Markatos, 'Computer simulation of multi- phase flows; a course of lectures and workshops', *CFD/83/4, CFDU*, Imperial College, University of London, 1983.
12. M. R. Malin and D. B. Spalding, 'A two-fluid model of turbulence and its application to heated plane jets and wakes', *PCH J.*, **5**, 339 (1984).
13. T. L. Cook and F. H. Harlow, 'VORT: a computer code for bubbly two- phase flow', *Los Alamos National Laboratory, LA-10021-MS*, 1984.
14. J. H. Hills, 'Radial non-uniformity of velocity and voidage in a bubble column', *Trans. Inst. Chem. Eng.*, **52**, 1–9 (1974).
15. A. Seriwaza, I. Kataoka and I. Michiyoshi, 'Phase distribution in bubbly flow: Data Set No. 24', in G. F. Hewitt, J. M. Delhaye and N. Zuber (eds), *Multiphase Science and Technology*, Vol. 6, Hemisphere, Washington, DC, 1992, p. 257.
16. J. T. Kuo and G. B. Wallis, 'Flow of bubbles through nozzles', *Int. J. Multiphase Flow*, **14**, 547 (1988).
17. G. B. Wallis, 'The terminal speed of single drops or bubbles in an infinite medium', *Int. J. Multiphase Flow*, **1**, 491 (1974).
18. T. L. Cook and F. H. Harlow, 'Virtual mass in multiphase flow', *Int. J. Multiphase Flow*, **10**, 691 (1984).
19. D. A. Drew and T. J. Lahey, 'The virtual mass and lift force on a sphere in rotating and straining inviscid flow', *Int. J. Multiphase Flow*, **13**, 113 (1987).
20. R. T. Lahey, 'The analysis of phase separation and phase distribution phenomena using two-fluid models', *Nucl. Eng. Design*, **122**, 17 (1990).
21. R. Kowe, J. C. R. Hunt, A. Hunt, B. Couet and L. J. S. Bradbury, 'The effects of bubbles on the volume fluxes and the pressure gradients in unsteady and non-uniform flow of liquids', *Int. J. Multiphase Flow*, **14**, 587 (1988).
22. T. Watanabe, M. Hirano, F. Tanabe and H. Kamo, 'The effect of the virtual mass force term on the numerical efficiency of system calculations', *Nucl. Eng. Design*, **120**, 181 (1990).
23. C. Prakash, 'Prediction of some complex multi-dimensional two-phase flow phenomena using the PHOENICS code', *Proc. 2nd Int. PHOENICS Users Conf.*, London, 1987.
24. S. W. Beyerlein, R. K. Crossmann and H. J. Richter, 'Prediction of bubble concentration profiles in vertical turbulent two-phase flow', *Int. J. Multiphase Flow*, **11**, 629 (1985).
25. A. D. Ciccone, J. G. Kawall and J. F. Keffer, 'On the determination of particle-erosion rates within a turbulent boundary layer', *Proc. 7th Symp. on Turbulent Shear Flows*, Stanford, CA, August 1989.
26. G. J. Lee and S. H. Chang, 'Physical modelling and finite-element method for the analysis of lateral phase distribution phenomena', *Int. Commun. Heat Mass Transfer*, **18**, 333 (1991).
27. M. Ishii, *Thermo-Fluid Dynamic Theory of Two-Phase Flow*, Eyrolles, Paris, 1975.
28. D. A. Drew, 'Mathematical modelling of two-phase flow', *Ann. Rev. Fluid Mech.*, **15**, 261 (1983).
29. J. H. Stuhmiller, 'The influence of interfacial pressure forces on the character of two-phase flow model equations', *Int. J. Multiphase Flow*, **3**, 551 (1977).
30. S. P. Antal, R. T. Lahey and J. E. Flaherty, 'Analysis of phase distribution in fully-developed laminar bubbly two-phase flow', *Int. J. Multiphase Flow*, **17**, 635 (1991).
31. S. T. Johansen and F. Boysan, 'Fluid dynamics in bubble-stirred ladles: Part II. Mathematical modelling', *Metall. Trans. B*, **19**, 755 (1988).
32. M. Lopez de Bertodano, S. J. Lee, R. T. Lahey and D. A. Drew, 'The prediction of two-phase turbulence and phase distribution phenomena using a Reynolds stress model', *ASME J. Fluids Eng.*, **112**, 107 (1990).
33. B. E. Launder and D. B. Spalding, 'The numerical computation of turbulent flows', *Comput. Methods Appl. Mech. Eng.*, **3**, 269 (1974).
34. W. Rodi, *Turbulence Models and Their Application in Hydraulics— A State of the Art Review*, IAHR, Delft, 1980.
35. M. R. Malin, 'Numerical simulation of two-phase flow in bubble columns', *CHAM Rep. 3311/1*, CHAM, London, 1995.
36. S. A. Morsi and A. J. Alexander, 'An investigation of particle trajectories in two-phase flow systems', *J. Fluid Mech.*, **55**, 193 (1972).

37. G. F. Hewitt, J. M. Delhaye and N. Zuber, 'Test 2.4, one-dimensional sedimentation', in G. F. Hewitt, J. M. Delhaye and N. Zuber (eds), *Multiphase Science and Technology*, Vol. 6, Hemisphere, Washington, DC, p. 623, 1992.
38. R. T. Lahey and M. Lopez de Bertodano, 'The prediction of phase distribution using two-fluid models', *ASME/JSME Thermal Eng. Proc.*, **2**, 193 (1991).
39. N. W. Rice and R. G. Geary, 'Prediction of liquid circulation in viscous bubble columns', *AIChE J.*, **36**, 1339–1348 (1990).